Two-dimensional plasma expansion in a magnetic nozzle: Separation due to electron inertia

Eduardo Ahedo and Mario Merino

Citation: Phys. Plasmas **19**, 083501 (2012); doi: 10.1063/1.4739791
View online: http://dx.doi.org/10.1063/1.4739791
View Table of Contents: http://pop.aip.org/resource/1/PHPAEN/v19/i8
Published by the American Institute of Physics.

Two-dimensional plasma expansion in a magnetic nozzle: Separation due to electron inertia

Eduardo Ahedo[a] and Mario Merino
Universidad Politécnica de Madrid, 28040 Madrid, Spain

(Received 12 April 2012; accepted 13 July 2012; published online 6 August 2012)

A previous axisymmetric model of the supersonic expansion of a collisionless, hot plasma in a divergent magnetic nozzle is extended here in order to include electron-inertia effects. Up to dominant order on all components of the electron velocity, electron momentum equations still reduce to three conservation laws. Electron inertia leads to outward electron separation from the magnetic streamtubes. The progressive plasma filling of the adjacent vacuum region is consistent with electron-inertia being part of finite electron Larmor radius effects, which increase downstream and eventually demagnetize the plasma. Current ambipolarity is not fulfilled and ion separation can be either outwards or inwards of magnetic streamtubes, depending on their magnetization. Electron separation penalizes slightly the plume efficiency and is larger for plasma beams injected with large pressure gradients. An alternative nonzero electron-inertia model [E. Hooper, J. Propul. Power **9**, 757 (1993)] based on cold plasmas and current ambipolarity, which predicts inwards electron separation, is discussed critically. A possible competition of the gyroviscous force with electron-inertia effects is commented briefly. © *2012 American Institute of Physics*. [http://dx.doi.org/10.1063/1.4739791]

I. INTRODUCTION

Divergent magnetic nozzles, created by longitudinal magnetic fields, are being envisaged as the acceleration stage of several advanced plasma thrusters.[1–5] In the highly competitive and demanding area of space propulsion, the optimization of plasma thruster characteristics (performances, weight, lifetime, etc.) is crucial. Thus, the eventual implementation of magnetic nozzles requires, among other aspects, a reliable and detailed understanding of the processes governing plasma expansion and thrust transmission. With this aim we developed in Ref. 1 a two-dimensional (2D) model of the expansion of a current-free, fully ionized, near-collisionless, hot plasma (as the one we expect to be delivered by the thruster chamber) in a magnetic nozzle (with no solid walls). We showed there that a *propulsive magnetic nozzle*, capable of increasing the thrust, requires a "hot" plasma, so that plasma internal energy is transformed into ion axial directed energy, and that the nozzle thrust transmission mechanism is the magnetic force of the azimuthal plasma current onto the thruster magnetic circuit.

As usual in analyses of magnetized plasma flows, our 2D model disregarded electron inertia effects, arguing that they were marginal. This was very beneficial for solving the model, since dropping convective terms makes electron momentum equations fully algebraic. In the zero electron-inertia limit, fully magnetized electrons are channeled perfectly by the magnetic field. On the contrary, for the expected magnetic intensities and propellants in envisaged thrusters, ions are only weakly magnetized (except perhaps for very light propellants). As a consequence, it was found that even fulfilling quasineutrality, ion streamtubes separate inwards from electron streamtubes, generating longitudinal electric currents and breaking current ambipolarity (CA).

The central motivation for discussing electron-inertia here is to analyze electron separation from the magnetic field as a step in understanding the downstream detachment of the plasma from the magnetic nozzle. In a low-beta plasma, the separation of strongly magnetized electrons from magnetic streamtubes can be achieved via resistivity or electron-inertia.[6] At least one of these mechanisms yields a *dominant term* in the equation determining the electron separation velocity. In a hot, fully ionized plasma, resistivity is weak and electron-inertia is likely to dominate electron separation. Furthermore, electron-inertia effects will be shown to be finite electron Larmor radius (FELR) effects[7]—here, finite meaning small but non-zero. Since the nozzle magnetic field decreases downstream, FELR effects increase and drive the process of plasma demagnetization, when the magnetically channeled plasma beam expands into the adjacent vacuum region. A linear perturbation analysis of the zero-inertia model[6] advanced that the electron fluid separates outwards from the magnetic lines. This will be confirmed by the model presented here, which accounts for nonlinear electron inertia.

Hooper,[10] working with a nonzero-inertia model, found inwards plasma separation. Since his model has been the basis for other works,[11–14] yielding inwards plasma separation too, a discussion of Hooper's model is very pertinent here. Hooper's model is similar to ours except for two important features, which are at the core of the disagreement with our conclusions: his model imposes current ambipolarity everywhere and is limited to the expansion of a cold plasma. In addition, Hooper applied his model only to a uniform, non-rotating beam at the nozzle throat. Schmit and Fisch[13] applied it to plasma beams with independent, nonzero

[a]Electronic addresses: eduardo.ahedo@upm.es. URL: web.fmetsia.upm.es/ep2 and mario.merino@upm.es. URL: web.fmetsia.upm.es/ep2.

azimuthal ion and electron flows. Little and Choueiri[14] have attempted to include the effects of plasma pressure in Hooper's model.

Electron-inertia is just one part of FELR effects. Full FELR effects include also the divergence of the gyroviscous (or stress) tensor,[7–9] known as gyroviscous force, which is ignored in all the above models. Consistent term ordering in plasma fluid models for the case of finite Larmor radius—discussed mainly in the plasma fusion field and focused on ions, but valid for electrons too—states that the gyroviscous force is of the order of the convective electron derivative in the so-called drift ordering.[7] Here, the possible competition of gyroviscous with electron-inertia effects will be only pointed out.

The rest of the paper is organized as follows. Section II recovers the model formulation for ions of Ref. 1. Section III derives and discusses the nonzero inertia model for the electron fluid. Section IV analyzes the plasma response in terms of main parameters. Section V discusses separately on current ambipolarity models and gyroviscous effects. Section VI compiles conclusions. A preliminary version of this work was presented as a conference paper.[15]

II. MODEL: NOZZLE AND ION EQUATIONS

The general assumptions and notation of the present model are identical to those in Ref. 1; only the elements that facilitate the autonomous reading of the present paper are repeated here. A current-free, fully ionized, collisionless plasma beam of radius R expands from the throat of a divergent magnetic nozzle created by a set of external coils and internal plasma currents. In the cylindrical frame of reference $\{\mathbf{1}_z, \mathbf{1}_r, \mathbf{1}_\theta\}$, with coordinates (z, r) for the axilsymmetric magnitudes, the total magnetic field is $\boldsymbol{B} = B(\mathbf{1}_z \cos\alpha + \mathbf{1}_r \sin\alpha)$. The convention $0 < \alpha < \pi/2$ is adopted for the local magnetic angle, and the magnetic reference $\mathbf{1}_\parallel = \boldsymbol{B}/B$ and $\mathbf{1}_\perp = \mathbf{1}_\theta \times \mathbf{1}_\parallel$ is used too. There exists a magnetic streamfunction, ψ, satisfying $\nabla\psi = rB\mathbf{1}_\perp$. For the simulations presented here, we will consider the applied magnetic field generated by a solenoid of radius $R_S = 3.5R$ and extending from $z = -2.5R$ to $z = 2.5R$, Fig. 1(a), and we will restrict the analysis to a low-density plasma so that the induced magnetic field is negligible (its inclusion can be carried out iteratively[16]). Thus, the throat is located at $z = 0$ and $\alpha(0, r) = 0$. Along the paper, subscript 0 will refer to values of magnitudes at $(z, r) = (0, 0)$.

A two-fluid model is used for the quasineutral plasma, with $n \equiv n_i = n_e$ being the plasma density. The general form of fluid equations for each plasma species ($j = i, e$) is

$$\nabla \cdot n_j \boldsymbol{u}_j = 0, \tag{1}$$

$$m_j n_j \boldsymbol{u}_j \cdot \nabla \boldsymbol{u}_j = -\nabla \cdot \boldsymbol{P}_j - q_j n_j \nabla\phi + q_j n_j \boldsymbol{u}_j \times \boldsymbol{B}, \tag{2}$$

where $\boldsymbol{u}_j$ is the species fluid velocity, $\boldsymbol{P}_j$ is the pressure tensor, and the rest of symbols is conventional. For vector magnitudes, such as velocities $\boldsymbol{u}_j$ ($j = i, e$) and current densities $\boldsymbol{j}_j$, their longitudinal (i.e., meridian) projections are denoted with a tilde: $\tilde{\boldsymbol{u}}_j = \boldsymbol{u}_j - u_{\theta j}\mathbf{1}_\theta$, etc.

The set of equations for ions can be expressed as

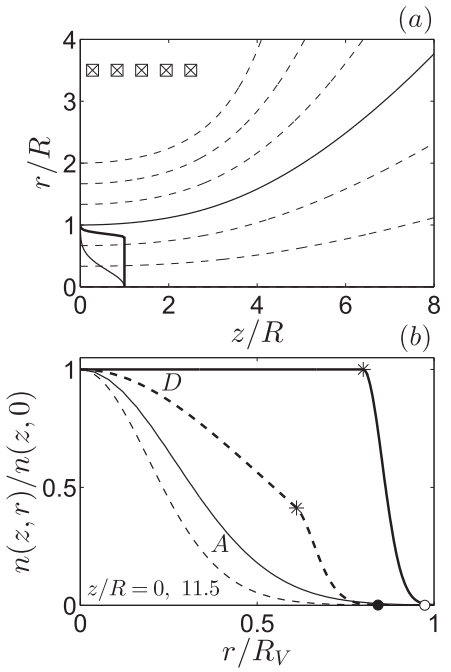

FIG. 1. (a) Magnetic field lines created by the solenoid (squares), and sketches of the two beam density profiles at the throat. The solid line corresponds to the nozzle edge $r = R_B(z)$ in the zero electron-inertia limit. (b) Density profiles at the throat and at section $z/R = 11.5$ for simulations A and D. Asterisks represent the border between the central and peripheral regions of simulation D. Circles represent the location of the magnetic nozzle edge $r = R_B(z)$ at $z/R = 11.5$ for simulations A (white) and D (black).

$$u_{ri}\frac{\partial \ln n}{\partial r} + u_{zi}\frac{\partial \ln n}{\partial z} + \frac{\partial u_{ri}}{\partial r} + \frac{\partial u_{zi}}{\partial z} = -\frac{u_{ri}}{r}, \tag{3}$$

$$u_{ri}\frac{\partial u_{ri}}{\partial r} + u_{zi}\frac{\partial u_{ri}}{\partial z} = -\frac{e}{m_i}\frac{\partial \phi}{\partial r} + u_{\theta i}\Omega_i \cos\alpha + \frac{u_{\theta i}^2}{r}, \tag{4}$$

$$u_{ri}\frac{\partial u_{zi}}{\partial r} + u_{zi}\frac{\partial u_{zi}}{\partial z} = -\frac{e}{m_i}\frac{\partial \phi}{\partial z} - u_{\theta i}\Omega_i \sin\alpha, \tag{5}$$

$$r m_i u_{\theta i} + e\psi = D_i(\psi_i), \tag{6}$$

where ϕ is the ambipolar electric potential, $\Omega_i = eB/m_i$ is the ion gyrofrequency, the ion pressure tensor has been neglected, ψ_i is the ion streamfunction, satisfying

$$\nabla\psi_j = -rn\tilde{\boldsymbol{u}}_j \times \mathbf{1}_\theta \tag{7}$$

(with $j = i$), and $D_i(\psi_i)$ is the total azimuthal momentum for ions in each streamline, which is determined from conditions at the throat.

In order to complete this set of equations, a relation between ϕ and n is needed, which will be provided by the electron model. Initial conditions (at $z = 0$, $r \le R$) for the above equations are the same as in previous works,

$$u_{ri} = 0, \quad u_{\theta i} = 0, \quad u_{zi} = c_s M_0, \tag{8}$$

with $M_0 \ge 1$, and $n(0, r)$ is provided; Fig. 1(b) shows the density profiles used in the simulations below. Notice that ions enter the diverging nozzle without rotation (or swirling). Ion swirling is known to occur in some devices[17] and has been proposed by Schmit and Fisch for increasing inwards plasma separation in the frame of Hooper's model.

III. MODEL: ELECTRON EQUATIONS

As in Ref. 1, let us consider a simple isotropic, isothermal model for the pressure tensor, i.e.,

$$\nabla \cdot \boldsymbol{P}_e \equiv T_e \nabla n_e. \tag{9}$$

Then because of axisymmetry and no resistivity, the azimuthal momentum equation reduces to

$$\frac{u_{re}}{r}\frac{\partial (r u_{\theta e})}{\partial r} + u_{ze}\frac{\partial u_{\theta e}}{\partial z} = \frac{eB}{m_e} u_{\perp e}. \tag{10}$$

It is evident that this equation determines $u_{\perp e}$, and yields $u_{\perp e} = 0$ in the limit $m_e/m_i \to 0$. Making use of the magnetic streamfunction, a first integral of Eq. (10) is

$$r m_e u_{\theta e} - e\psi = D_e(\psi_e), \tag{11}$$

where ψ_e is the electron streamfunction, satisfying Eq. (7) for $j = e$, and $D_e(\psi_e)$ is determined from throat conditions too. A second conservation law along electron streamtubes applies to the Bernoulli function,

$$T_e \ln n - e\phi + m_e(\tilde{u}_e^2 + u_{\theta e}^2)/2 = H_e(\psi_e), \tag{12}$$

with $H_e(\psi_e)$ also determined from throat conditions. The third scalar electron momentum equation is the projection along $\mathbf{1}_{\perp e} = \mathbf{1}_\theta \times \tilde{\boldsymbol{u}}_e/\tilde{u}_e$: substituting Eqs. (11) and (12) into Eq. (16) of Ref. 1 yields

$$u_{\theta e} D_e' = r H_e' + \frac{m_e}{n}\left(\kappa_e \tilde{u}_e - \frac{\partial \tilde{u}_e}{\partial \mathbf{1}_{\perp e}}\right), \tag{13}$$

where primes denote derivatives and κ_e is the meridian curvature of the electron streamtubes. Equations (11)–(13) are exact for the thermodynamic model of Eq. (9).

The electron massless model of Ref. 1 corresponds to the limit $m_e \to 0$ of Eqs. (11)–(13), which take well-known forms: Eq. (11) states that electron streamtubes are magnetic streamtubes and therefore yields $u_{\perp e} = 0$; Eq. (12) becomes the Boltzmann relation along electron streamtubes, with $-H_e/e$ the so-called "thermalized potential;" and Eq. (13) states, first, that $u_{\theta e}$ is the sum of $\boldsymbol{E}\times\boldsymbol{B}$ and $\nabla p \times \boldsymbol{B}$ drifts [Eq. (25) of Ref. 1], and, second, that the macroscopic azimuthal frequency is constant within streamtubes, that is,

$$\frac{u_{\theta e}}{r} \equiv w_{\theta e}(\psi_e) = -\frac{H_e'}{D_e'}, \tag{14}$$

a property known as isorotation.[18] In addition, for a current-free plasma, we infer that $u_{\parallel e} \sim \tilde{u}_e \sim \tilde{u}_i \sim c_s$, whereas the value of $u_{\theta e}$ is closely dependent on the shape of $n(0, r)$. A typical range would be $O(c_s) \le u_{\theta e} \le O(c_e)$ with $c_e = \sqrt{T_e/m_e}$.[1]

In a collisionless plasma, electron-inertia effects constitute the only contribution making $u_{\perp e}$ different from zero. Hence, an electron model retaining the dominant contribution of *every* component of $\boldsymbol{u}_e$ must keep the whole equation (11) or the equivalent Eq. (10). On the contrary, the terms with $m_e\tilde{u}_e$ in Eqs. (12) and (13) yield only a contribution of $O(m_e/m_i)$ in $u_{\parallel e}$ and $u_{\theta e}$, and therefore can be dropped. Summarizing, the proposed nonzero-inertia electron model consists of Eqs. (11), (14), and

$$T_e \ln n - e\phi = H_e(\psi_e) - m_e r^2 w_{\theta e}^2(\psi_e)/2. \tag{15}$$

This model retains fully azimuthal inertia and neglects longitudinal one. Mathematically, the withdrawal of the inertia term in Eq. (13) keeps electron momentum equations algebraic, a very positive feature to be exploited next.

Equation (15) provides the relation between n and ϕ required by Eqs. (3)–(6). However, it also involves the electron streamfunction $\psi_e(z, r)$. Since now $u_{\perp e} \neq 0$, electron streamtubes separate from magnetic streamtubes and their shape must be determined from Eq. (11). Substituting Eq. (14) into it yields

$$r^2 m_e w_{\theta e}(\psi_e) - e\psi(z, r) = D_e(\psi_e), \tag{16}$$

which is an implicit equation for $\psi_e(z, r)$. Therefore, Eqs. (15) and (16) complete the set of equations (3)–(6). Substituting the derivatives of ϕ, Eqs. (3)–(5) constitute a set of three hyperbolic equations for $M_0 > 1$ that are integrated with the method of characteristics of Ref. 1.

The magnetic and electron streamtubes that depart from $(z, r) = (0, R)$ define, respectively, the magnetic nozzle edge, $r = R_B(z)$, and the plasma beam edge, $r = R_V(z)$; their shapes are obtained from solving $\psi(0, R) = \psi(z, R_B)$ and $\psi_e(0, R) = \psi_e(z, R_V)$. Since $R_V \equiv R_B$ for $m_e/m_i \to 0$, the difference between the magnetic and beam edges measures the electron separation caused by azimuthal electron inertia. The beam edge delimits an ideal plasma/vacuum boundary. In order to minimize the effect of an artificial pressure jump there, we will consider initial density profiles decaying to near-zero at the edge; specifically, we will take $n(0, R) = 10^{-3} n_0$.

Equation (16) establishes a principal feature of our electron model: electron streamtubes and their separation from magnetic streamtubes depend exclusively on the magnetic topology and electron conservation laws, and are independent of the ion dynamics and the plasma density map. From Eqs. (7) and (16), the slope of the electron streamtubes is

$$\frac{u_{re}}{u_{ze}} = -\frac{\partial \psi_e/\partial z}{\partial \psi_e/\partial r} = \frac{eB\sin\alpha}{eB\cos\alpha - 2m_e w_{\theta e}}. \tag{17}$$

This yields a second central feature: electron separation from magnetic streamtubes depends exclusively on the sign of $w_{\theta e}(\psi_e)$, which is determined by the beam conditions at the throat. Assuming a steady-state plasma beam inside the cylindrical source upstream of the divergent nozzle, Tonks[19,20] showed that the azimuthal electron current is always diamagnetic, which means $w_{\theta e} > 0$ (for our convention on α). Therefore, under that general equilibrium condition, one has

$$u_{re}/u_{ze} > \tan\alpha \tag{18}$$

and the electron streamtubes separate *outwards* from the magnetic streamtubes.

Furthermore, in the strong magnetization limit, the upstream plasma equilibrium corresponds to a θ-pinch,[21]

where the expanding plasma pressure gradient is balanced by the confining magnetic force generated by the azimuthal plasma current, while the confining electric force is negligible. In fact, the θ-pinch limit of Tonks is adopted here as the radial electron equilibrium at the throat

$$0 = -T_e \frac{\partial \ln n}{\partial r} - e u_{\theta e} B + \frac{m_e u_{\theta e}^2}{r}. \tag{19}$$

The last, "centrifugal" term is small (and partially artificial, as we will comment later) but it is kept for the mathematical consistency of our fluid model. For $n(0, r)$ given, Eq. (19) determines the distribution of angular velocities,

$$w_{\theta e}(\psi_e(0,r)) \simeq -\left[\frac{T_e}{eBr}\frac{\partial \ln n}{\partial r}\right]_{z=0}.$$

According to Eq. (17), the magnitude of the electron/magnetic separation is proportional to $w_{\theta e}/\Omega_e$, with $\Omega_e = eB/m_e$ the local electron gyrofrequency. Near the throat and for $\partial \ln n/\partial r \sim 1/R$, one has $w_{\theta e}/\Omega_e \sim (\ell_{e0}/R)^2$, which shows that electron-inertia effects are indeed FELR effects. Since $w_{\theta e}$ is conserved in the electron streamtubes, electron-inertia effects grow downstream as $w_{\theta e}/\Omega_e \propto B^{-1} \propto R_B^2$, as predicted in Ref. 6.

To complete the electron model, the electron initial longitudinal velocity must be defined. Here, we will impose current ambipolarity locally at the throat,

$$\tilde{\boldsymbol{u}}_e(0,r) = \tilde{\boldsymbol{u}}_i(0,r). \tag{20}$$

IV. DISCUSSION OF RESULTS

A. Plasma expansion features

The current parametric investigation is limited to the shape of the initial density profile, $n(0, r)$, and two dimensionless parameters, m_e/m_i and $\hat{\Omega}_{i0} = \Omega_{i0}R/c_s$. As an alternative to one of them, the FELR parameter $\hat{\ell}_{e0} = \ell_{e0}/R = \sqrt{m_e/m_i}\hat{\Omega}_{i0}^{-1}$ can be used. The rest of parameters of the model was discussed in previous works and they have no major relevance on the discussion here. Table I summarizes the five simulations illustrated in the figures to come. Initial density profiles are depicted in Fig. 1(b): simulations O to C correspond to a plasma beam with $w_{e0}(0,r) = \text{const}$, yielding a near-Gaussian density profile,

$$n(0,r) = n_0 \exp\left[\frac{-2e w_{\theta e}\psi + m_e w_{\theta e}^2 r^2}{2T_e}\right]; \tag{21}$$

and simulation D corresponds to an initially near-uniform beam, treated in Subsection IV B.

Figure 2 illustrates electron and ion separation for simulations A and B, which operate with the same gas (i.e., same m_e/m_i) and different magnetic intensity B_0. As discussed before, electron separation is outwards and it increases as the magnetic field decreases. The ambipolar electric force caused by quasineutrality tends to keep the ion streamtubes close to the electron ones. However, the incomplete ion magnetization makes them separate inwards from the electron streamtubes, except at the plasma/vacuum edge $r = R_V(z)$. Here lies a key difference with Hooper's class of models, which tie *a priori* ion and electron streamtubes. Let $\alpha_{jB} = \text{angle}(\boldsymbol{B}, \tilde{\boldsymbol{u}}_j)$ $(j = i, e)$, be the separation angles of ion and electron streamtubes with respect to the magnetic field. Figure 3 plots examples of the possible behaviors: $\alpha_{eB} = 0$ and $\alpha_{iB} < 0$, for $m_e/m_i = 0$; $\alpha_{eB} > 0$ and α_{iB} taking both signs; and $\alpha_{eB} > 0$ and $\alpha_{iB} > 0$. Simulations A and C operate with different gases but share the same magnetic intensity. This means the electron separation is the same in both cases, but ion streamtubes are (slightly) more divergent for light hydrogen ions than for heavy xenon ions.

Interestingly, in the zero-inertia limit ion separation is always inwards, i.e., $\alpha_{iB} < 0$. This implies that $u_{\theta i}$ is positive (for a plasma source yielding a negligible ion swirl current), so that the ion azimuthal current is paramagnetic and contributes negatively to the thrust.[1] For $m_e/m_i \neq 0$, the ion azimuthal current can take both signs within the plasma beam and its contribution to thrust is less negative. Anyway, this

TABLE I. Parameters of the different simulations presented in the figures. Simulation *O* corresponds to the zero electron inertia limit. Simulations *A* and *B* differ in the magnetic intensity. Simulations *A* and *C* differ in the propellant. Simulations *A* and *D* differ in the initial density profiles, which are defined within the main text. All simulations take $M_0 = 1.05$ to ensure Eqs. (3)–(5) are hyperbolic.

Simulations	$\hat{\ell}_{e0}$	Ions	$\hat{\Omega}_{i0}$	n profile
O	0	…	0.409	Gaussian-like
A	5×10^{-3}	Xe^+	0.409	Gaussian-like
B	5×10^{-2}	Xe^+	0.0409	Gaussian-like
C	5×10^{-3}	H^+	4.67	Gaussian-like
D	5×10^{-3}	Xe^+	0.409	Uniform-like

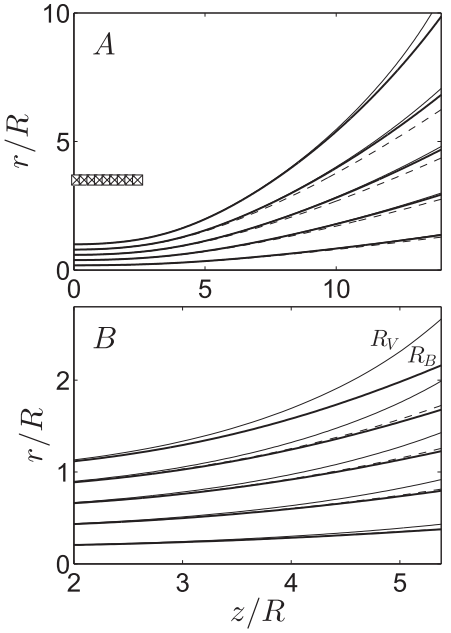

FIG. 2. Streamtubes of magnetic field (solid, thick), electrons (solid, thin), and ions (dashed) for simulations A and B. Each group of 3 lines starts from the same location at $z = 0$, thus showing the downstream electron and ion separation from the magnetic field. R_V and R_B represent the beam and nozzle edges, respectively. The electron separation of simulation A is the same as that of *C*. Notice the different axes scales.

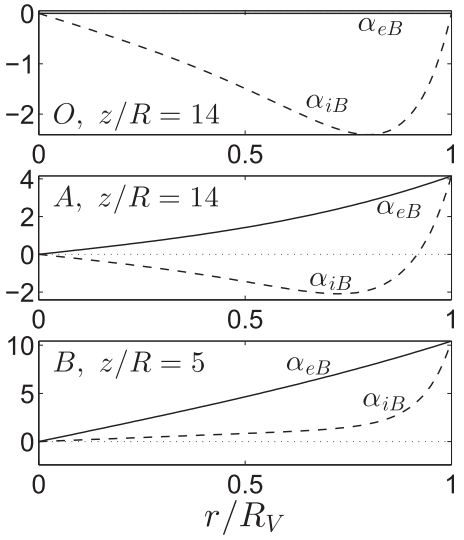

FIG. 3. Examples of local separation angles (in degrees) of electron (solid) and ion (dashed) streamtubes from the magnetic streamtubes in different simulations and at different locations (as indicated on each plot). Electron separation is always outwards; ion separation can be outwards or inwards.

contribution is marginal in all practical cases. Inwards ion separation has been observed in several recent experiments.[22–25] Outwards ion separation, which requires outwards electron separation, has been observed too.[25]

The outwards separation of electron streamtubes implies that a stronger radial electric field is needed to pull ions towards the more divergent beam edge and satisfy quasineutrality there. The correlation of electron separation and radial fall of the electric potential is evident in the profiles of simulations A and B in Fig. 4. The difference between simulations A and C is due to the different ion mass: lower electric fields are necessary to push lighter ions radially.

Figure 5 plots the local plume efficiency, $\eta_{plume}(z)$. This was defined in Eq. (49) of Ref. 1 as the ratio P_{zi}/P_z of the axial flows of axial versus total ion energy at sections $z=\text{const}$. We observe that electron inertia penalizes η_{plume} since the beam divergence increases, but the penalty is small since the large radial rarefaction leaves a very small beam density at the edge vicinity.

The electron inertia effects analyzed here do not modify the limits of validity of our plasma model, which were set already in Ref. 1. The model fails downstream because of (a) electron demagnetization, measured by ℓ_e/R, or (b) loss of

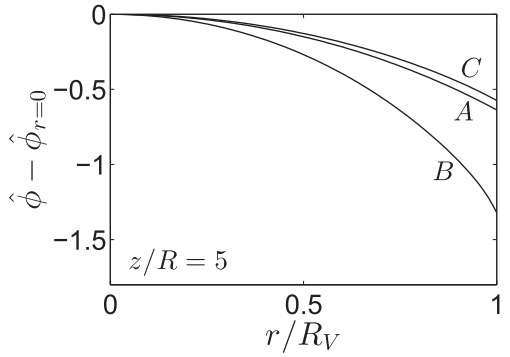

FIG. 4. Radial profile of electric potential at $z/R=5$ for simulations A, B, and C; $\hat{\phi}=e\phi/T_e$.

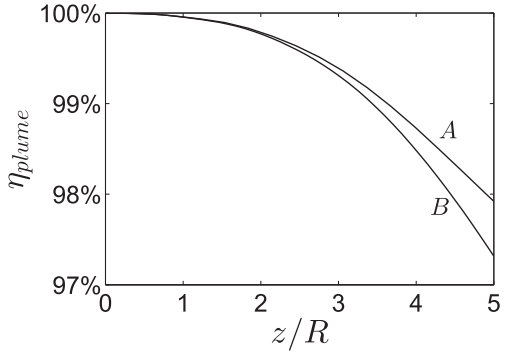

FIG. 5. Plume efficiency variation along z for simulations A and B. Plume efficiency for simulation C (not shown here) is practically identical to simulation A.

electron confinement, measured by $\tilde{u}_e/c_e$. Figure 6(a) illustrates the increase of ℓ_e/R caused by the decrease of magnetic intensity in a divergent topology. Figure 6(b) plots $\tilde{u}_e^2/c_e^2$; the increase of this parameter downstream (and mainly near the plasma edge) is caused by electron flux conservation under the large plasma rarefaction.[1] Since the relative contribution of electron longitudinal inertia to $u_{\theta e}$ in Eq. (13) is $O(\tilde{u}_e^2/c_e^2)$ roughly [see Section III], there is no additional restriction to the validity of the present nonzero-inertia model. To confirm this last trend, Fig. 6(c) plots constant-level lines of the ratio of the second versus the first term on

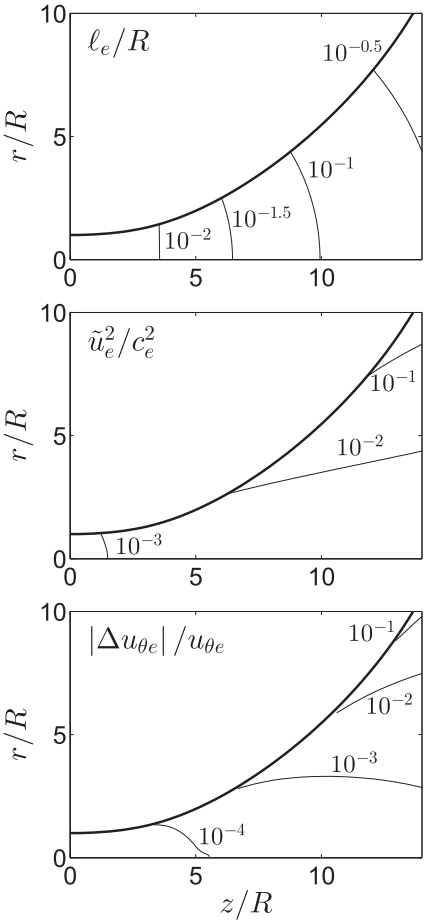

FIG. 6. 2D maps for simulation C of: (a) electron gyroradius parameter, (b) longitudinal electron velocity parameter, and (c) relative contribution of electron longitudinal inertia to $u_{\theta e}$ in Eq. (13).

the right-hand-side of Eq. (13). Additionally, since these two terms have different signs, we conclude that longitudinal inertia decreases $u_{\theta e}$ (and thus breaks isorotation). Finally, we note that, for simulation A, which uses xenon instead of hydrogen, the curves of Figs. 6(b) and 6(c) correspond to values two orders of magnitude lower, while Fig. 6(a) coincides.

B. Near-uniform beam at the throat

A uniform density profile of the injected plasma beam [i.e., $n(0,r) = \text{const} = n_0$] is often used in 2D studies of magnetic nozzles.[10,26] That profile presents a strong discontinuity at the plasma-vacuum edge that must be discussed. In Ref. 1, we demonstrated that, in the limit $\ell_e/R \to 0$, the discontinuity is in fact a layer of $O(\ell_e)$-thickness, where a large azimuthal electron current develops so that the resulting magnetic force balances the plasma pressure jump. Furthermore, since the azimuthal electron current is zero within the uniform beam, the electron current at the edge becomes then the *main* contribution to thrust from the magnetic nozzle.

Electron-inertia effects imply that $\ell_{e0}/R \neq 0$ and make it impossible to maintain the above two-scale analysis. In order to tackle the uniform-profile case within a one-scale analysis, here we consider a profile of $n(0, r)$, which is uniform until a certain radius R_1 close to R, and then decays exponentially to almost zero. Figure 1(b) plots the particular profile simulated here, with $R_1 = 0.8R$. There is a double interest in simulating a near-uniform profile. The first one is to validate the results of the two-scale analysis of Ref. 1 and to extend them beyond the asymptotic limit $\ell_e/R \to 0$. The second one is that a near-uniform profile highlights particular features of the expansion and separation of the plasma beam, thus casting additional light on the subject.

Figures 1(b) and 7 plot the profiles of density and azimuthal electron current, respectively, at $z/R = 0$ and 11.5 for the case of a near-uniform density profile at the throat; the Gaussian-profile case is included for comparison. For the near-uniform case, the plasma beam in the nozzle can be divided into central and peripheral regions, separated by the magnetic streamtube departing from $r = R_1$, that is

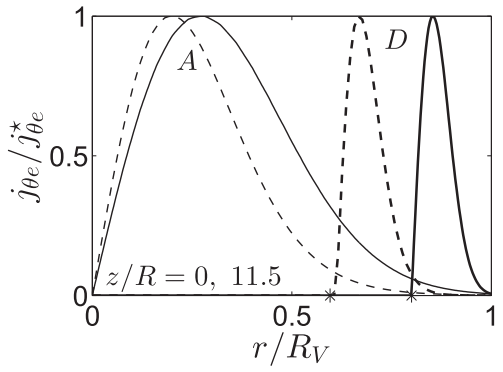

FIG. 7. Azimuthal electron currents (normalized with maximum value of each curve) for simulations A (thin) and D (thick). The dimensionless peak values are 5.46 at $z = 0$ (solid) and 0.34 at $z/R = 11.5$ (dashed) in simulation A, and 26.6 at $z = 0$ and 0.71 at $z/R = 11.5$ in simulation D. Asterisks correspond to the same points of Fig. 1(b).

$\psi(z,r) = \psi(0,R_1)$, marked with asterisks in the figures. The set of Eqs. (14) and (19) states that $u_{\theta e} = 0$ in the whole central region, which is illustrated in Fig. 7. Therefore, in the central region there is no electron separation and no magnetic force: the electron pressure gradient observed in Fig. 1(b) is balanced only by the electric force. On the contrary, the plasma behavior in the peripheral region is qualitatively identical to the one found before for the Gaussian density profile, as Figs. 1(b) and 7 illustrate too. An interesting feature is that the separation of the electron streamtubes is larger the more uniform the initial profile is (i.e., as R_1/R is closer to one), because the larger pressure gradient $[\sim T_e n_0/(R - R_1)]$ requires a larger $u_{\theta e}$, which in turn yields a larger $u_{\perp e}$. The circles in Fig. 1(b) correspond to $r = R_B$ for $z/R = 11.5$, thus showing the magnitude of the separation of the electron streamtube.

V. DISCUSSION OF MODEL ASSUMPTIONS

A. On current ambipolarity models

The local CA condition is

$$\tilde{\boldsymbol{u}}_i - \tilde{\boldsymbol{u}}_e = 0. \tag{22}$$

Since our model satisfies

$$\nabla \cdot en(\tilde{\boldsymbol{u}}_i - \tilde{\boldsymbol{u}}_e) = 0, \tag{23}$$

imposing CA at the throat section, condition (20), is enough to assure that the plasma beam is current-free in the whole nozzle, that is

$$\int_0^{R_V(z)} drrn(u_{zi} - u_{ze}) = 0, \quad \forall z. \tag{24}$$

The imposition of CA is natural in quasi-1D models, where it is equivalent to the current-free condition, but in our 2D *diverging* nozzle model, local CA is not fulfilled in any volume, *independently* of both boundary conditions and electron-inertia effects. As discussed in Ref. 1, the nonfulfilment of CA is an *immediate* consequence of the separation between electron and ion streamtubes, which is possible thanks to the partial magnetization of ions and the ambipolar electric field preserving quasineutrality. Furthermore, Figs. 7(c) and 8(c) of Ref. 1 illustrated that imposing CA either at the throat or at a downstream section, CA is not fulfilled in the rest of nozzle sections.

Although electron-inertia effects have little to do with CA fulfilment, they have been a central piece in the formulation of Hooper's model.[10] We are now able to show that this model is mathematically inconsistent and yields nonphysical solutions. Notice first, that our 2D model involves 8 independent scalar equations for 8 scalar variables: $\boldsymbol{u}_i$, $\boldsymbol{u}_e$, n, and ϕ. Clearly, none of the particle and momentum equations is dispensable; also, although the equations are coupled among them, it is possible to identify which plasma variable is determined preferentially by each equation.

Hooper applies Eq. (22) instead of Eq. (23). This substitution adds one extra equation to the problem, making it incompatible, as we show next. The set of equations (4)–(6)

plus Eq. (10) *substituting* $u_{\perp e}$ with $u_{\perp i}$ is *complete* for the four variables $\tilde{\boldsymbol{u}}_i$, and $u_{\theta e}$ in a cold plasma. Notice that the modified Eq. (10)—or Eq. (11)—determines $u_{\theta e}$. Apart from these four equations, Eq. (3) would yield n. Still there are the two electron longitudinal momentum equations, (14) and (15), to be satisfied but only one variable, ϕ, remains undetermined. The incompatibility of this CA model lies in that Eq. (14) *also* determines $u_{\theta e}$—stating it to be the well known $(en\boldsymbol{E}+\nabla p_e)\times\boldsymbol{B}$ drift. Clearly, the over-determined character of the model would be avoided by just removing the CA condition and letting Eq. (10) to determine $u_{\perp e}(\neq u_{\perp i})$, as we do.

We can venture the reasons why Hooper, in an otherwise well-reasoned and clearly presented paper, did not detect the model inconsistency. The first reason is that, although he was well aware that CA is just an approximation in a 2D model (he devotes a whole section to discuss CA) he supposed the approximation to be a good one. The second reason is that an omission on the manipulation of the equations rendered his CA model mathematically compatible. To explain it, let us first write Eqs. (14) and (15) in the compact form

$$0=\nabla\left[T_e\,\ln n-e\phi+\frac{1}{2}m_e u_{\theta e}^2\right]-\frac{u_{\theta e}}{r}\frac{dD_e}{d\psi_e}\nabla\psi_e. \qquad (25)$$

Hooper's error was to treat the function $D_e(\psi_e)$ ($-e\Psi_0$ in his notation) as a constant, when, both in the general case and in his application to a uniform beam with $u_{\theta e}(0,r)=0$, it is not. That mistake leads to the omission of the last term of Eq. (25): this term (divided by m_e) is missed in Eq. (11) of Hooper,[10] in Eq. (2.8) of Schmit and Fisch,[13] and in Eqs. (8) and (9) of Little and Choueiri.[14] The maimed version of equation (25) yields only one scalar equation: $H_e(\psi_e)=$ const, and misses completely the indispensable Eq. (14). The "vacancy" left by Eq. (14) was supplanted by imposing CA, leading to a model mathematically compatible but ill-derived and nonphysical.

The nonphysical aspects of Hooper's model can be discussed in terms of the electric potential. First, his cold plasma satisfies a limit form of Eq. (15): $e\phi-m_e u_{\theta e}^2/2=0$, Eq. (12) of Ref. 10. This implies that ϕ is minimum at the axis and grows radially, indeed pushing electrons radially outwards, fully opposed to a typical plasma expansion. Second, the nature of the electric field in the cold plasma model, responsible of keeping quasineutrality and 2D current ambipolarity, is very uncertain. Schmit and Fisch speculate on the presence of "local microscopic ambipolar electric fields," while "no macroscopic self-field can arise in the system." But our hot-plasma (quasineutral) model shows, first, that the ambipolar electric field is proportional to T_e, and second, the pressure contribution can never be dropped, even downstream, since it always dominates over the ambipolar electric force. This is true also for an adiabatic electron pressure law, instead of an isothermal one, and for a plasma beam injected at high supersonic velocities, i.e., M_0 large, a case approaching Hooper's one, and commented in Ref. 6.

Consequently, the cold-plasma case is not a regular limit of the hot-plasma model. Furthermore, as the plasma becomes more supersonic, the perpendicular electric field and plasma rarefaction become larger. This weakens plasma quasineutrality and supports the idea that the electric field in the cold-plasma limit is of non-neutral character, generated by the space-charge being built between weakly magnetized ions trying to move axially and electrons trying to follow the divergent magnetic lines. The idea of electrostatic separation as a detachment mechanism of the far-downstream plasma was raised in Ref. 6.

Little and Choueiri[14] have extended Hooper's model to a hot plasma, adding the pressure contribution to their equations for the longitudinal velocity of the electron-ion pair. Apart from using an approximate continuity equation to determine n, the main objection here is that, as Hooper, they integrate the resulting equations along the well-tied electron-ion streamlines, and they maintain the mathematical omission in Eq. (25). Instead, our ion equations (3)–(5) take $\phi(n)$ from the electron model and are integrated along the classical three families of characteristics lines of an expanding hot gas: ion streamlines and the pair of Mach lines.[1]

Our conclusion is that the failure of CA and thus the presence of longitudinal currents are inherent to the 2D divergent expansion of a plasma beam with partially magnetized ions. Furthermore, we believe it to be fundamental for downstream plasma detachment.[6] CA would be fulfilled in the ion strong-magnetization limit, defined as $\Omega_i R/c_s\to\infty$, when ion streamtubes coincide with electron and magnetic streamtubes. But the ion strong-magnetization limit is not appropriate for magnetic intensities and propellants used in plasma thrusters.[1] Besides, even if that limit is applicable at the throat region, it eventually fails downstream.

The presence of longitudinal currents raises the issue of the current closure, which was already commented in Ref. 1 and continues open. A reliable answer requires both to extend the 2D nozzle model far downstream and to match it upstream with a plasma source model. One presumes that for the plasma beam injecting into a weak environmental plasma, a far downstream current closure across the magnetic field can be postulated. Also, if the plasma beam impinges on a conducting plate, this will host the current closure path. However, if the beam impinges on an absorbing or recombining insulating surface—like in Fig. (8c) of Ref. 1—the current closure is expected to happen upstream, in the more-collisional plasma source.

B. On full FELR effects

The electron-inertia hot-plasma model discussed hereto assumes the simplest form of the pressure tensor of Eq. (9): $\boldsymbol{P}_e$ is diagonal, isotropic, and isothermal. Non-isothermality is easy to take into account and leads mainly to a qualitative change on the far plasma response. Pressure anisotropy, with different parallel and perpendicular temperatures, is of interest for certain plasma thrusters, in particular the electrodeless electron cyclotron resonance thruster.[11,27] Non-isothermality and anisotropy are dominant (i.e., zero-Larmor-radius) effects on the electron response and require an independent study.

On the contrary, the non-diagonal part of the pressure tensor, Π_e, known as the stress or gyroviscous tensor[7–9]

defines the gyroviscous force, $G = \nabla \cdot \Pi_e$, which is a finite Larmor-radius effect. In the present case, where electron-inertia effects are limited to the azimuthal momentum equation, Eq. (10), only the component G_θ could be relevant. Although recognizing its importance, the evaluation of the gyroviscous force is a challenge which merits a dedicated work. The first difficulty is that there is no consensus on the expression of the gyroviscous force, although Ramos[9] has derived recently a general (and extremely involved) expression of it, which, in different limits, recovers cases of other authors. In particular, for a near-Maxwellian electron velocity distribution function with temperature T_e, the gyroviscous force would reduce to Braginski's expression,[8] which is Eq. (28) of Ref. 9.

Focusing now on that expression, the second challenge is that the gyroviscous force includes several terms, which can be grouped on two types. On the one hand, there are linear terms on first-order derivatives of $\boldsymbol{u}_e$ and p_e, which would provide a *partial diamagnetic cancellation* of electron inertia.[7] For instance, they would cancel the small "centrifugal force" in Eq. (19) and would oppose (but may not cancel) the convective radial derivative of Eq. (10). On the other hand, there is the true viscous contribution, consisting of terms with second order derivatives of $\boldsymbol{u}_e$ and products of first-order derivatives of $\boldsymbol{u}_e$ and p_e. These terms break the hyperbolicity of the ion equations, making our current integration approach inapplicable.

Since the gyroviscous force is proportional to $T_e/eB_0 \equiv (\ell_{e0}/R)^2$, given B_0 it vanishes, together with the pressure, only in the cold plasma case. For the case of interest of a hot-plasma in a diverging nozzle, the suitable expression of the gyroviscous force and the relative ordering of its different terms has to be assessed. This will indicate whether there is a parametric range where the gyroviscous force can dominate FELR effects.

VI. CONCLUSIONS

Electron-inertia constitutes a mechanism capable of detaching highly magnetized electrons from nozzle magnetic streamtubes. Electron-inertia effects are part of finite electron-Larmor radius effects. Therefore, they increase downstream, as the magnetic strength decreases, and constitute a sign of plasma demagnetization.

Here, dominant electron-inertia effects have been studied within an isothermal fluid model. The electron momentum equations reduce to three algebraic laws, stating conservation of the Bernoulli function and the azimuthal momentum, and isorotation along electron streamtubes. As a consequence, the shape of the electron streamtubes and thus their separation from magnetic streamtubes becomes independent of the ion dynamics. This electron model yields, under rather general equilibrium conditions on the injected plasma beam, that electrons separate outwards of the magnetic lines, the plasma beam thus progressively filling the vacuum region adjacent to the nozzle, which is coherent with FELR effects leading to plasma demagnetization.

While electron separation depends mainly on the electron Larmor radius, ion separation depends on both the ion Larmor radius (based on the directed velocity) and the ambipolar perpendicular electric field (affected by electron separation). Both inwards and outwards ion separation from the magnetic lines can take place, as it has been observed experimentally. As long as the FELR parameter is small, it penalizes only slightly the plume efficiency. When, farther downstream, the FELR parameter becomes of order one, the plasma demagnetizes, but this nozzle region is out of the limits of the present model.

A study of near-uniform beams at the throat has confirmed a previous two-scale study for the zero electron gyroradius limit and makes more evident the role of the azimuthal electron current on the force balance and the plasma separation, which is larger in plasma beams injected with large pressure gradients.

A dissection of Hooper's model, which yields inwards electron separation, has been undertaken in order to understand the cause of our mutual disagreement. It has been demonstrated that: (1) forcing current ambipolarity everywhere leads to an incompatible model, where $u_{\theta e}$ is determined simultaneously from two independent equations; (2) a term was erroneously omitted in the manipulation of the equations, with important consequences on the resulting model; and (3) the electric potential presents a nonphysical profile and its ambipolar character—justifying a quasineutral model—is uncertain in his cold plasma.

It is concluded that the failure of current ambipolarity is natural in the diverging expansion of a meso-magnetized plasma and possibly fundamental for its downstream detachment, but we acknowledge that the upstream and downstream current closures remain an issue to be studied. For the future, a dedicated analysis of the gyroviscous force—very scarcely studied in the plasma propulsion context—seems convenient. This force could compete with electron inertia and completes FELR effects on a hot, collisionless plasma. However, the gyroviscous force could ruin the hyperbolicity of our equations, invalidating our efficient and successful integration scheme for the plasma/nozzle problem.

ACKNOWLEDGMENTS

This work has been sponsored by the Air Force Office of Scientific Research, Air Force Material Command, USAF, under Grant No. FA8655-12-1-2043. The U.S. Government is authorized to reproduce and distribute reprints for Governmental purpose notwithstanding any copyright notation hereon. Additional support for this research was provided by the Gobierno de España (Project AYA-2010-61699).

[1]E. Ahedo and M. Merino, "Two-dimensional supersonic plasma acceleration in a magnetic nozzle," Phys. Plasmas **17**, 073501 (2010).
[2]E. Ahedo, "Plasmas for space propulsion," Plasma Phys. Controlled Fusion **53**, 124037 (2011).
[3]G. Krülle, M. Auweter-Kurtz, and A. Sasoh, "Technology and application aspects of applied field magnetoplasmadynamic propulsion," J. Propul. Power **14**, 754–763 (1998).
[4]C. Diaz, "The VASIMR rocket," Sci. Am. **283**(5), 90–97 (2000).
[5]R. Winglee, T. Ziemba, L. Giersch, J. Prager, J. Carscadden, and B. R. Roberson, "Simulation and laboratory validation of magnetic nozzle effects for the high power helicon thruster," Phys. Plasmas **14**, 063501 (2007).

[6]E. Ahedo and M. Merino, "On plasma detachment in propulsive magnetic nozzles," Phys. Plasmas **18**, 053504 (2011).
[7]R. D. Hazeltine and F. L. Waelbroeck, *The Framework of Plasma Physics* (Perseus Books, 2004).
[8]S. I. Braginskii, in *Reviews of Plasma Physics, Volume 1*, edited by M. A. Leontovich (Consultants Bureau, New York, 1965) p. 205.
[9]J. J. Ramos, "General expression of the gyroviscous force," Phys. Plasmas **12**, 112301 (2005).
[10]E. B. Hooper, "Plasma detachment from a magnetic nozzle," J. Propul. Power **9**(5), 757–763 (1993).
[11]J. C. Sercel, "Simple model of plasma acceleration in a magnetic nozzle," in *AIAA, DGLR, and JSASS, 21st International Electric Propulsion Conference*, AIAA Paper No. 90-2597, 1990.
[12]D. A. Kaufman, D. G. Goodwin, and J. C. Sercel, "Plasma separation from magnetic field lines in a magnetic nozzle," in *31st AIAA Aerospace Sciences Meeting and Exhibit*, AIAA Paper No. 93-0817, 1993.
[13]P. F. Schmit and N. J. Fisch, "Magnetic detachment and plume control in escaping magnetized plasma," J. Plasma Phys. **75**(03), 359–371 (2009).
[14]J. M. Little and E. Y. Choueiri, "The influence of induced currents on magnetic nozzle acceleration and plasma detachment," in *Proceedings of 46th Joint Propulsion Conference, Nashville, TN* (American Institute of Aeronautics and Astronautics, Washington DC, 2010), AIAA Paper No. 2010-6615.
[15]E. Ahedo and M. Merino, "On electron inertia and current ambipolarity in magnetic nozzle models," in *32nd International Electric Propulsion Conference, Wiesbaden, Germany* (Electric Rocket Propulsion Society, Fairview Park, OH, 2011), IEPC Paper No. 2011-050.
[16]M. Merino and E. Ahedo, "Plasma detachment mechanisms in a magnetic nozzle," in *Proceedings of 47th Joint Propulsion Conference, San Diego, CA* (American Institute of Aeronautics and Astronautics, Washington DC, 2011), AIAA Paper No. 2011-5999.
[17]D. B. Fradkin, A. W. Blackstock, D. J. Roehling, T. F. Stratton, M. Williams, and K. W. Liewer, "Experiments using a 25-kw hollow cathode lithium vapor mpd arcjet," AIAA J. **8**, 886–894 (1970).
[18]S. Chandrasekhar, "Axisymmetric magnetic fields and fluid motions," Astrophys. J. **124**, 232–243 (1956).
[19]L. Tonks, "Theory of magnetic effects in the plasma of an arc," Phys. Rev. **56**, 360–373 (1939).
[20]E. Ahedo, "Parametric analysis of a magnetized cylindrical plasma," Phys. Plasmas **16**, 113503 (2009).
[21]J. Freidberg, *Plasma Physics and Fusion Energy* (Cambridge University Press, Cambridge, 2007).
[22]W. Cox, C. Charles, R. W. Boswell, and R. Hawkins, "Spatial retarding field energy analyzer measurements downstream of a helicon double layer plasma," Appl. Phys. Lett. **93**, 071505 (2008).
[23]K. Terasaka, S. Yoshimura, K. Ogiwara, M. Aramaki, and M. Y. Tanaka, "Experimental studies on ion acceleration and stream line detachment in a diverging magnetic field," Phys. Plasmas **17**, 072106 (2010).
[24]K. Takahashi, Y. Itoh, and T. Fujiwara, "Operation of a permanent-magnets-expanding plasma source connected to a large-volume diffusion chamber," J. Phys. D: Appl. Phys. **44**, 015204 (2011).
[25]J. P. Squire, C. S. Olsen, F. R. C. Díaz, L. D. Cassady, B. W. Longmier, M. G. Ballenger, M. D. Carter, T. W. Glover, and G. E. McCaskill, "VASIMR® vx-200 operation at 200 kw and plume measurements: Future plans and an iss ep test platform," in *32nd International Electric Propulsion Conference, Wiesbaden, Germany* (Electric Rocket Propulsion Society, Fairview Park, OH, 2011), IEPC Paper No. 2011-154.
[26]A. V. Arefiev and B. N. Breizman, "Magnetohydrodynamic scenario of plasma detachment in a magnetic nozzle," Phys. Plasmas **12**, 043504 (2005).
[27]W. M. Manheimer and R. F. Fernsler, "Plasma acceleration by area expansion," IEEE Trans. Plasma Sci. **29**, 75–84 (2001).